Solid-State NMR, Crystallographic and Density Functional Theory Investigation of Fe−CO and Fe−CO Analogue Metalloporphyrins and Metalloproteins[†]

Renzo Salzmann,[‡] Michael T. McMahon,[⊥] Nathalie Godbout, Lori K. Sanders, Mark Wojdelski,[§] and Eric Oldfield*

Contribution from the Departments of Chemistry and Biophysics, University of Illinois at Urbana-Champaign, 600 South Mathews Avenue, Urbana, Illinois 61801

Received September 14, 1998. Revised Manuscript Received February 12, 1999

Abstract: We have synthesized and characterized the following four metalloporphyrins: Fe(OEP)(CO)-(1-MeIm), Ru(OEP)(CO)(1-MeIm), Os(OEP)(CO)(1-MeIm), and Fe(TPP)(iPrNC)(1-MeIm), where OEP = 2,3,7,8,12,13,17,18-octaethylporphyrinate, TPP = 5,10,15,20-tetraphenylporphyrinate, and 1-MeIm = 1-methylimidazole, using single-crystal X-ray diffraction, solid-state nuclear magnetic resonance (NMR), and density functional theory (DFT) methods. Unlike the situation found with the Fe-, Ru-, Os(TPP)(CO)(1-MeIm) analogues, which have ruffled porphyrins, all four systems here have essentially planar porphyrin rings, and a rule is developed that successfully predicts the presence or absence of ring distortion in a broad range of metalloporphyrins. In each of the three CO complexes, the M−C−O bond is close to linear and untilted, but with the iPrNC adduct, there are noticeable ligand distortions supporting the idea that RNC groups (but not CO) may be distorted in metalloproteins. Solid-state ^{13}C, ^{15}N, and ^{17}O NMR shifts and shift tensors determined experimentally are in generally good agreement with those computed via DFT. For isocyanide binding to proteins, the experimental shifts are more deshielded than in the model system, and the effects which might contribute to this difference are explored theoretically. Unlike CO, electrostatic field effects are unlikely to make a major contribution to protein shielding. Neither are Fe−C−N tilt−bend distortions, although a bend at nitrogen is energetically feasible and also gives a large deshielding, as seen with proteins.

Introduction

The preferential binding of O_2 over CO by the metalloproteins hemoglobin and myoglobin and the structural features which contribute to this discrimination have been topics of debate for some time.[1−10] The interest arises from the fact that CO binds much less strongly to these proteins than it does to unhindered metalloporphyrin model compounds, a fortunate circumstance since CO is produced in vivo as a product of porphyrin catabolism. A variety of mechanisms have been postulated for this discrimination, ranging from a protein-induced distortion of the Fe−C−O bond[11] to hydrogen-bonding stabilization of bound O_2 by the distal ligand[12−14] and the closely related hydrogen bonding/water binding model.[10,14] In addition, metalloporphyrin distortions have been reported in some heme proteins,[15] and can also be expected to influence ligand binding. However, the precise nature of these stabilizing/destabilizing effects has been difficult to evaluate at the molecular level, since the protein structures themselves are part of the debate.[16] There is, therefore, interest in employing spectroscopic methods to study structure and bonding in metalloproteins, using well-characterized model systems to help make the structure-spectroscopic correlations, which should then form the basis for further structure refinements of proteins themselves, both in solution and in the crystalline solid-state. As an example of this approach, we recently reported the synthesis and characterization of a series of carbonmonoxymetalloporphyrins[17] which

(1) Pauling, L.; Coryell, C. D. *Proc. Natl. Acad. Sci. U.S.A.* **1936**, *22*, 210−216.

(2) Pauling, L. *Nature* **1964**, *203*, 182−183.

(3) Weiss, J. J. *Nature* **1964**, *203*, 182−183.

(4) Jameson, G. B.; Molinaro, F. S.; Ibers, J. A.; Collman, J. P.; Brauman, J. I.; Rose, E.; Suslick, K. S. *J. Am. Chem. Soc.* **1978**, *100*, 6769−6770. Collman, J. P.; Gagne, R. R.; Reed, C. A.; Robinson, W. T.; Rodley, G. A. *Proc. Natl. Acad. Sci. U.S.A.* **1974**, *71*, 1326−1329.

(5) Sage, J. T. *J. Biol. Inorg. Chem.* **1997**, *2*, 537−543.

(6) Slebodnick, C.; Ibers, J. A. *J. Biol. Inorg. Chem.* **1997**, *2*, 521−525.

(7) Lim, M.; Jackson, T. A.; Anfinrud, P. A. *J. Biol. Inorg. Chem.* **1997**, *2*, 531−536.

(8) Spiro, T. G.; Kozlowski, P. M. *J. Biol. Inorg. Chem.* **1997**, *2*, 516−520.

(9) Spiro, T. G.; Kozlowski, P. M. *J. Am. Chem. Soc.* **1998**, *120*, 4524−4525.

(10) Olson, J. S.; Phillips, G. N., Jr. *J. Biol. Inorg. Chem.* **1997**, *2*, 544−552.

(11) Kuriyan, J.; Wilz, S.; Karplus, M.; Petsko, G. A. *J. Mol. Biol.* **1986**, *192*, 133−154. Stryer, L. *Biochemistry*; W. H. Freeman and Co.: New York, 1995.

(12) Phillips, S. E. V.; Schoenborn, B. P. *Nature* **1981**, *292*, 81−82.

(13) Nagai, K.; Luisi, B.; Shih, D.; Miyazaki, G.; Imai, K.; Poyart, C.; DeYoung, A.; Kwiatkowsky, L.; Noble, R. W.; Lin, S.-H.; Yu, N.-T. *Nature* **1987**, *329*, 858−860.

(14) Springer, B. A.; Sligar, S. G.; Olson, J. S.; Phillips, G. N., Jr. *Chem. Rev.* **1994**, *94*, 699−714.

(15) Shaanan, B. *J. Mol. Biol.* **1983**, *171*, 31−59.

(16) Ray, G. B.; Li, X.-Y.; Ibers, J. A.; Sessler, J. L.; Spiro, T. G. *J. Am. Chem. Soc.* **1994**, *116*, 162−176.

(17) Salzmann, R.; Ziegler, C. J.; Godbout, N.; McMahon, M.; Suslick, K. S.; Oldfield, E. *J. Am. Chem. Soc.* **1998**, *120*, 11323−11334.

proved to be useful in analyzing nuclear magnetic resonance (NMR), Mössbauer, and infrared (IR) spectroscopic data on CO-heme proteins.[18-20] Interestingly, in that work[17] we noted that there were pronounced rufflings for each of the three metalloporphyrins containing 1-methylimidazole as an axial base, while all three species containing axial pyridine ligands were essentially planar.[17]

In this work, we have extended the earlier study[17] to encompass different porphyrin ring substituents, as well as a different (but isoelectronic) axial ligand, isopropylisocyanide (iPrNC), to see experimentally what effects changes in ring and axial substitutions have on structure. We have synthesized and characterized four new compounds: the octaethylporphyrin (2,3,7,8,12,13,17,18-octaethylporphyrinate = OEP) adducts Fe-(OEP)(CO)(1-MeIm), Ru(OEP)(CO)(1-MeIm), and Os(OEP)-(CO)(1-MeIm), which unlike the TPP analogues we find to be planar rather than ruffled, and the isocyanide adduct Fe(TPP)-(iPrNC)(1-MeIm) (TPP = 5,10,15,20-tetraphenylporphyrinate), which unlike the CO TPP derivative is also found to contain a planar porphyrin—although the RNC group is noticeably distorted, as are several RNC—protein adducts.[21,22] These new compounds, together with the O_2-analogue species described in the following article,[23] form an interesting series of compounds with which to study how porphyrin ring substitutions and axial ligands can influence porphyrin distortions, a topic more typically limited to metal and porphyrin ring substitutions,[24] but which may also be of importance in metalloprotein function. An empirical rule is developed which enables the correct prediction of the presence or absence of porphyrin ruffling for 16 out of 16 systems, containing TPP, OEP, CO, CCl_2, RNC, RNO, py, or 1-MeIm ligands. We also report and investigate via density functional theory the solid-state NMR of these four new compounds, together with an analysis of the potential energy surfaces for Fe—RNC distortion. This provides information on the extent to which the alkylisocyanides can be distorted in proteins, analogous to previous work on CO-containing metalloporphyrin model systems,[18-20] and complementary to the work reported on heme protein isocyanide systems by Mims et al.,[25] but using a quantum chemical approach.

(18) Godbout, N.; Havlin, R.; Salzmann, R.; Debrunner, P. G.; Oldfield, E. *J. Phys. Chem. A* **1998**, *102*, 2342−2350.

(19) Havlin, R. H.; Godbout, N.; Salzmann, R.; Wojdelski, M.; Arnold, W.; Schulz, C. E.; Oldfield, E. *J. Am. Chem. Soc.* **1998**, *120*, 3144−3151.

(20) McMahon, M. T.; deDios, A. C.; Godbout, N.; Salzmann, R.; Laws, D. D.; Le, H.; Havlin, R. H.; Oldfield, E. *J. Am. Chem. Soc.* **1998**, *120*, 4784−4797.

(21) Johnson, K. A.; Olson, J. S.; Phillips, G. N., Jr. *J. Mol. Biol.* **1989**, *207*, 459−463. Johnson, K. A. Thesis, Rice University, 1993. Eich, R. F.; Li, T.; Lemon, D. D.; Doherty, D. H.; Curry, S. R.; Aitken, J. F.; Mathews, A. J.; Johnson, K. A.; Smith, R. D.; Phillips, G. N., Jr.; Olson, J. S. *Biochemistry* **1996**, *35*, 6976−6983.

(22) Johnson, K. A.; Olson, J. S.; Smith, R. D.; Phillips, G. N., Jr. *Protein Data Bank in Crystallographic Databases−Information Content, Software Systems, Scientific Applications*; Data Commission of the International Union of Crystallography; file nos. 101m, 103m, 104m, 105m, 106m, 107m, 108m, 109m, 110m, 111m, 112m, 2hbc, 2hd, 2hbe, 2hbf, 2mya, 2myb, 2myc, 2myd, and 2mye.

(23) Godbout, N.; Sanders, L. K.; Salzmann, R.; Havlin, R. H.; Wodjelski, M.; Oldfield, E. *J. Am. Chem. Soc.* **1999**, *121*, 3829.

(24) Sparks, L. D.; Medforth, C. J.; Park, M.-S.; Chamberlain, J. R.; Ondrias, M. R.; Senge, M. O.; Smith, K. M.; Shelnutt, J. A. *J. Am. Chem. Soc.* **1993**, *115*, 581−592. Munro, O. Q.; Bradley, J. C.; Hancock, R. D.; Marques, H. M.; Marsicano, F.; Wade, P. W. *J. Am. Chem. Soc.* **1992**, *114*, 7218−7230. Scheidt, W. R.; Lee, Y. J. *Struct. Bonding (Berlin)*, **1987**, *64*, 1−70.

(25) Mims, M. P.; Olson, J. S.; Russu, I. M.; Miura, S.; Cede, T. E.; Ho, C. *J. Biol. Chem.* **1983**, *258*, 6125−6134.

Experimental Section

Synthetic Aspects. The synthesis of Fe(OEP)(CO)(1-MeIm), Ru-(OEP)(CO)(1-MeIm), and Os(OEP)(CO)(1-MeIm) followed the basic protocols outlined previously for the synthesis of Fe(TPP)(CO)-(1-MeIm), Ru(TPP)(CO)(1-MeIm), and Os(TPP)(CO)(1-MeIm),[17] and will not be further elaborated on, except that the Fe(OEP)(CO)(1-MeIm) crystals were grown from hexane/benzene while the Ru, Os derivatives were from methylene chloride/methanol. Analytical data for Fe(OEP)-(CO)(1-MeIm)•0.5hexane: Elemental Anal. Found (Calculated): C, 70.89 (71.23); H, 7.91 (7.75); N, 10.88 (11.33). IR (ν_{CO} in CH_2Cl_2): 1965 cm^{-1}. ^{13}C NMR (CO): 206.9 ppm. Ru(OEP)(CO)(1-MeIm)•CH_2-Cl_2: Elemental Anal. Found (Calculated): C, 60.73 (60.86); H, 6.31 (6.33); N, 9.97 (10.14). IR (ν_{CO} in CH_2Cl_2): 1924 cm^{-1}. ^{13}C NMR (CO): 182.8 ppm. Os(OEP)(CO)(1-MeIm)•CH_2Cl_2: Elemental Anal. Found (Calculated): C, 54.99 (54.95); H, 5.67 (5.71); N, 8.97 (9.15). IR (ν_{CO} in CH_2Cl_2): 1893 cm^{-1}. ^{13}C NMR (CO): 141.2 ppm. For solid-state NMR experiments, we used ^{13}CO, $C^{17}O$, [2-N^{13}C] propane and [2-^{15}NC] propane axial ligands, the labeled isopropylisocyanides being synthesized from 2-iodopropane and labeled AgCN basically as described elsewhere.[26]

(2-Isocyanopropane)(1−methylimidazole)(5,10,15,20-tetraphenylporphyrinato)iron(II) and (2-Isocyanopropane)(pyridine)-(5,10,15,20-tetraphenylporphyrinato)iron(II). The syntheses of both of these isopropylisocyanide Fe TPP adducts were carried out with use of the following procedure: Five milliliters of THF was degassed with Ar for 10 min in a 15 mL Schlenk flask equipped with a magnetic stirring bar, followed by 4 freeze−pump−thaw cycles. Fifty milligrams of (octaethylporphyrin)Fe^{III}Cl was then added under Ar counterflow, followed by ca. 2 equiv of $NaBH_4$. The Schlenk was then closed and stirred for 45 min on an open Ar line. 2.2 equivalents of pyridine or 1-MeIm were than added under Ar and the system closed and stirred for 1 h. The bis(1-MeIm) complex gives a metallic purple precipitate while the bis-py complex is orange and soluble. THF was then completely removed under high vacuum. Three milliliters $CHCl_3$ (previously degassed) was then added and the solutions transferred via cannula to a 100 mL Schlenk flask, to which was added a 10-fold excess of 2-isocyanopropane. The solutions were stirred for 20 h, then a 10-fold excess of pentane (degassed) was added dropwise to form a 2-layer system, from which the corresponding isocyanide adducts crystallized after several days. Fe(TPP)(iPrNC)(1-MeIm)•0.5pentane: Elemental Anal. Found (Calculated): C, 76.91 (76.48); H, 5.41 (5.54); N, 11.30 (11.45).

All compounds were fully characterized by field desorption mass spectrometry, UV−visible absorption, and solution and solid-state NMR spectroscopy. Elemental analyses were conducted in the University of Illinois School of Chemical Sciences Microanalytical Laboratory. Field desorption mass spectrometry measurements were carried out by using a Finnigan-MAT (Bremen, Germany) Model 731 instrument. Porphyrin UV−visible spectra were measured with use of a Hitachi Ltd. (Tokyo, Japan) Model 3300 UV−visible double monochromator spectrophotometer. The single-crystal X-ray measurements were made on a Siemens (Madison, WI) SMART diffractometer. Solid-state NMR spectra were obtained on "home-built" 360 and 500 MHz spectrometers, using Oxford magnets (Oxford Instruments, Oxford, UK), Tecmag (Houston, TX) data systems, and Doty Scientific (Columbia, SC) probes.

Crystallographic Aspects. Single-crystal data for the three systems described above were collected on a Bruker (Madison, WI) SMART/CCD diffractometer using Mo Kα radiation (λ = 0.71073 Å). The structures were solved by using the SHELXTL V5.0 (Bruker) system and refined by full-matrix least squares on F^2. Hydrogen atoms were assigned idealized locations and given isotropic thermal parameters 1.2 times the thermal parameter of the atom to which they were attached. The data were corrected for Lorentz and polarization effects, and an empirical absorption correction was applied.

(26) Jackson, H. L.; McKusick, B. C. In *Organic Synthesis*; Cairns, T. L., Cason, J., Johnson, W. S., Leonard, N. J., Newman, M. S., Price, C. C., Sheehan, J. C., Eds.; John Wiley & Sons: New York, 1955; Vol. 35, pp 62−64.

Table 1. Crystallographic Data Summary

	Fe(OEP)(CO)(1-MeIm)	Ru(OEP)(CO)(1-MeIm)	Os(OEP)(CO)(1-MeIm)	Fe(TPP)(iPrNC)(1-MeIm)
formula	$C_{41}H_{50}N_6OFe\bullet$ hexane	$C_{41}H_{50}N_6ORu\bullet$ methylene chloride	$C_{41}H_{50}N_6OOs\bullet$ methylene chloride	$C_{53}H_{41}N_7Fe\bullet$ 0.5pentane
formula weight	741.81	828.87	918.00	855.84
color	red	red	dark red	black
crystal system	triclinic	triclinic	triclinic	triclinic
a (Å)	11.872(2)	10.4568(2)	10.3677(3)	10.9981(7)
b (Å)	13.192(3)	12.98060(10)	12.9871(4)	13.2076(8)
c (Å)	14.305(3)	15.9683(2)	15.9564(5)	17.1650(11)
α (deg)	84.19(3)	80.6950(10)	80.6350(10)	73.86
β (deg)	69.72(3)	76.9820(10)	76.7310(10)	78.0500(10)
γ (deg)	69.85(3)	72.0180(10)	72.2190(10)	79.5640(10)
V (Å^3)	1972.5(7)	1998.65(5)	1981.25(10)	2322.9(3)
Z	2	2	2	2
D_{calc} (g cm^{-3})	1.249	1.377	1.539	1.224
space group	$P\bar{1}$	$P\bar{1}$	$P\bar{1}$	$P\bar{1}$
radiation, wavelength (Å)	Mo Kα, 0.71073 Å	Mo Kα, 0.71073 Å	Mo Kα, 0.71073 Å	Mo Kα, 0.71073 Å
μ (mm^{-1})	0.424	0.567	0.339	0.369
crystal size (mm)	0.23 × 0.16 × 0.08	0.12 × 0.12 × 0.10	0.11 × 0.09 × 0.01	0.26 × 0.17 × 0.08
temp (K)	198(2)	198(2)	198(2)	198(2)
diffractometer	Bruker SMART/CCD	Bruker SMART/CCD	Bruker SMART/CCD	Bruker SMART/CCD
no. of data points collected	10326	13046	10705	11376
no. of data points with $I > 2\sigma(I)$	6785	9023	6919	7147
abs min/max	0.847/0.930	0.673/0.569	0.656/0.959	0.825/1.00
$R_1{}^a$ (obsd data)	0.059	0.059	0.065	0.0663
$wR_2(a,b)^b$	0.128 (0.061, 0.924)	0.122 (0.037, 4.960)	0.123 (0.025, 17.037)	0.160 (0.072, 3.968)
GOF^c	1.026	1.142	1.147	1.078

^{a} $R_1 = \sum(||F_o| - |F_c||)/\sum(|F_o|)$. ^{b} $wR_2 = [\sum[w(F_o{}^2 - F_c{}^2)^2]/\sum[w(F_o{}^2)^2]]^{1/2}$ where $w = 1/[\sigma^2(F_o{}^2) + (a*P)^2 + b*P]$ and $P = (F_o{}^2 + 2F_c{}^2)/3$. ^{c} GOF $= S = [\sum[w(F_o{}^2 - F_c{}^2)^2]/(n - p)]$ where n = the number of reflections and p = the total number of parameters refined.

The color and morphology of the crystals, the crystallographic systems, and space groups, and other information related to the crystal structure determinations, are summarized in Table 1. In general, from 10 326 to 13 046 data points were collected with the area detector, and from 6785 to 9023 data points having $I > 2\sigma(I)$ were used in the refinements. The final R1 values varied from 0.059 to 0.066 and the GOF values varied from 1.026 to 1.147, Table 1. (See also Supporting Information.) Atomic coordinates, bond lengths, angles, and thermal parameters have also been deposited with the Cambridge Crystallographic Data Centre (CCDC). Any request to the CCDC for this material should quote the full literature citation and the reference number.

Computational Section. The computational methods used here are very similar to the density functional theory (DFT) methods we have used elsewhere,[18−20] where numerous studies of the effects of functionals and basis sets on metal and ligand shieldings, and on metal electric field gradients (EFGs), were described. For investigating electrostatic field effects on ^{13}C, ^{15}N shielding, we used the [FeCNMe](2e) species shown in Figure 1A, which is basically that used by deDios and Earle[27] in their study of electrostatic field perturbations of the [FeCO](2e) species, where the minus signs (Figure 1A) represent 0.4e point charges, incorporated to maintain a low-spin d^6 Fe ground state.[27] For calculations of the effects of ligand tilt and bend on the computed shieldings, we used the Fe(bis(amidinato))(MeNC)(1-methylimidazole) model, which is based on the CO derivative used previously in our study of Fe−C−O distortion, and is essentially that used by several other groups[28−30] to deduce, e.g., tilt−bend energy surfaces for both Fe−C−O and Fe^{III}−C−N. In both sets of calculations, we used the sum-over-states density functional perturbation theory in its LOC1 approxi-
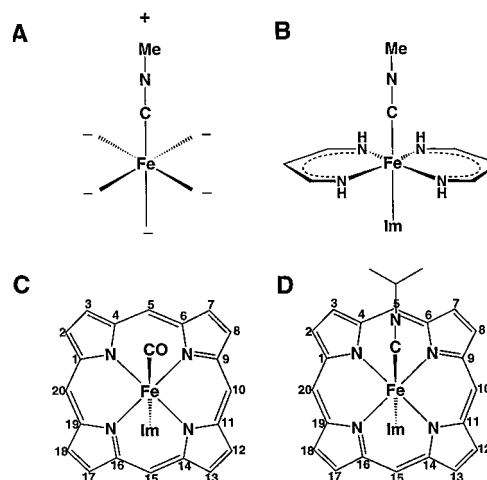

Figure 1. Schematic illustrations of the various structures used in the DFT calculations. (A) [FeCNMe](2e)(+) cluster used to evaluate the electrostatic contributions to shielding, as discussed by de Dios and Earle (ref 27). (B) Fe bis(amidinato)(CNMe)(Im) molecule used to evaluate ^{13}C, ^{15}N axial ligand shifts and energetics as a function of tilt (τ), C-bend (β), and N-bend (θ). (C) Basic M(P)(CO)(1-MeIm) structure used for ^{13}C, ^{17}O shielding calculations, using the bond lengths and bond angles derived crystallographically. (D) Fe(P)(iPrNC)(1-MeIm) structure used for ^{13}C, ^{15}N shielding calculations, using the bond lengths and bond angles derived crystallographically for Fe(TPP)(iPrNC)(1-MeIm).

(27) deDios, A. C.; Earle, E. M. *J. Phys. Chem. A* **1997**, *101*, 8132−8134.

(28) Strich, A.; Veillard, A. *Theor. Chim. Acta* **1981**, *60*, 379−383.

(29) Jewsbury, P.; Yamamoto, S.; Minato, T.; Saito, M.; Kitagawa T. *J. Am. Chem. Soc.* **1994**, *116*, 11586−11587. Jewsbury, P.; Yamamoto, S.; Minato, T.; Saito, M.; Kitagawa, T. *J. Phys. Chem.* **1995**, *99*, 12677−12685.

(30) Vangberg, T.; Bocian, D. F.; Ghosh, A. *J. Biol. Inorg. Chem.* **1997**, *2*, 526−530. Ghosh, A.; Bocian, D. F. *J. Phys. Chem.* **1996**, *100*, 6363−6367.

mation[31] using individual gauges for localized orbitals[32] as implemented in the deMon program.[33] We used Wachters' all electron basis set for

(31) Malkin, V. G.; Malkina, O. L.; Casida, M. E.; Salahub, D. R. *J. Am. Chem. Soc.* **1994**, *116,* 5898−5908. Salahub, D. R. In *Theoretical and Computational Chemistry*; Politzer, P., Seminario, J. M., Eds.; Elsevier: New York, 1995.

(32) Kutzelnigg, W.; Fleischer, U.; Schindler M. In *NMR−Basic Principles and Progress*; Springer: Heidelberg, 1990; Vol. 28, p 1965.
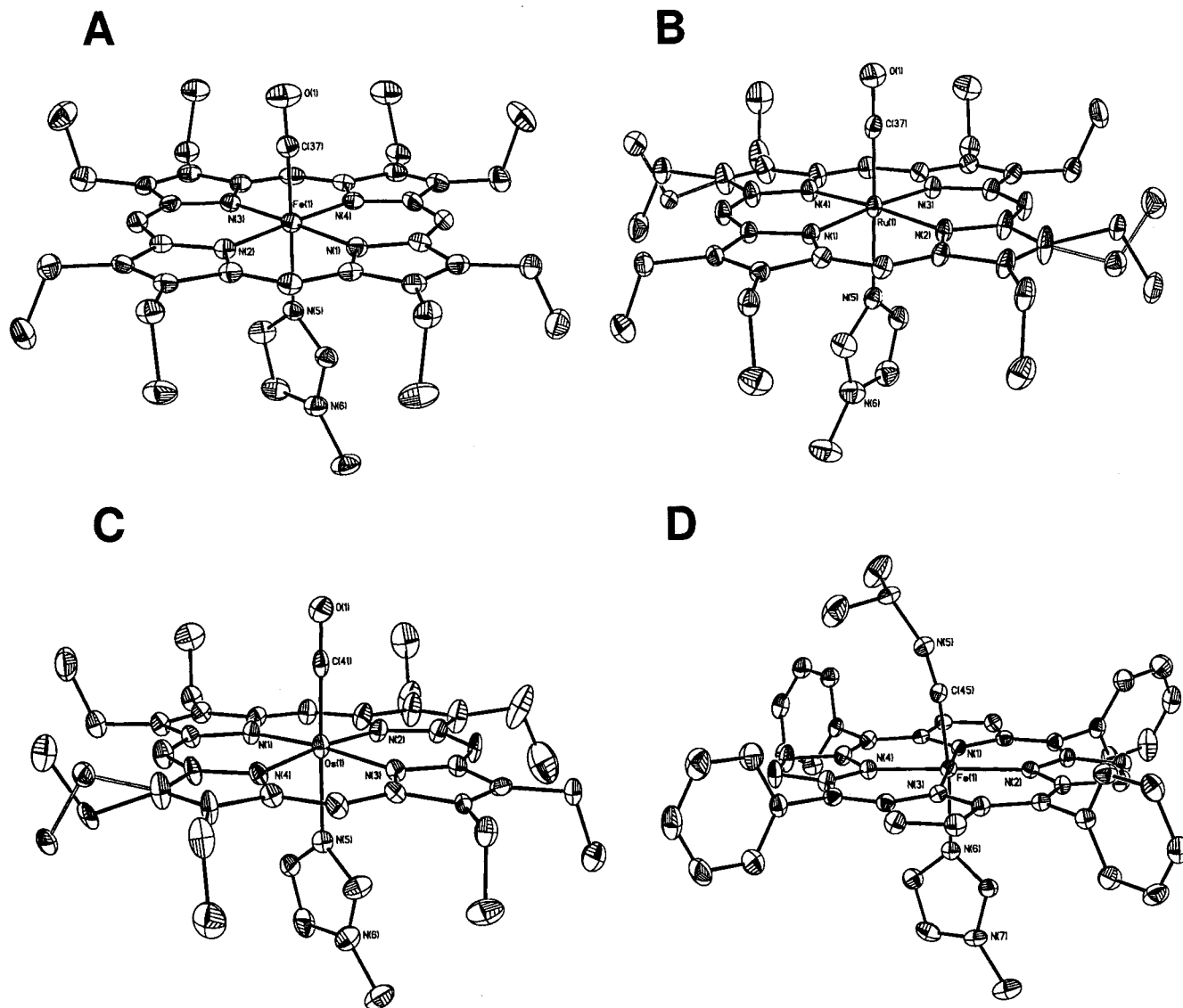
A

B

C

D

Figure 2. SHELXTL (Bruker, 1998) X-ray structures of the four compounds investigated. (A) Fe(2,3,7,8,12,13,17,18-octaethylporphyrinate)(CO)-(1-methylimidazole); (B) Ru(2,3,7,8,12,13,17,18-octaethylporphyrinate)(CO)(1-methylimidazole); (C) Os(2,3,7,8,12,13,17,18-octaethylporphyrinate)-(CO)(1-methylimidazole); and (D) Fe(5,10,15,20-tetraphenylporphyrinate)(2-isocyanopropane)(1-methylimidazole). The representations show 35% probability ellipsoids for non-H atoms. H atoms were omitted for clarity. Ethyl group disorder is present in parts B and C.

iron (14s9p5d/8s5p5d),[34,35] an IGLO-II basis for H,C,N, together with the Perdew-Wang (PW91) gradient-corrected exchange-correlation functional.[36] The electrostatic field perturbations were generated by the presence of point charges of varying magnitudes at 4.45 Å from the isocyanide N, along the Fe−C−N axis. We also performed a second set of calculations using the FeCO(2e) model and a point charge of varying magnitude at 4.45 Å from the carbonmonoxy O, along the Fe−C−O axis, for direct comparison with the isocyanide results.

For the ^{13}C, ^{15}N, and ^{17}O shielding calculations on the three metalloporphyrins, we employed the Gaussian-94/DFT/GIAO program[37] as described previously.[18−20] We used our experimental X-ray structures but minus the porphyrin ring substituents (i.e., Ph, Et → H, refs 18−20), which does not affect ligand shielding, together with a Wachters' basis on Fe, 6-311++G(2d) on the attached porphyrin nitrogens, the metal coordinated nitrogen of the axial base and the isocyanide C and N, 6-31G* on all porphyrin carbons attached to nitrogen, and 3-21G* elsewhere. The same scheme was used for the carbon monoxide complexes. For the Ru and Os compounds, we employed the same scheme as that described previously,[17] in which the metals are represented with effective or model core potentials (ECPs).[37] This locally dense[38] approach has been used and tested previously[18−20] and gives good accord with experiment. The BPW91 exchange correlation

(33) Salahub, D. R.; Fournier, R.; Mlynarski, P.; Papai, I.; St.-Amant, A.; Ushio, J. In *Density Functional Methods in Chemistry;* Labanowski, J., Andzelm, J., Eds.; Springer: New York, 1991. St.-Amant, A.; Salahub, D. R. *Chem. Phys. Lett.* **1990**, *169*, 387−392.

(34) Wachters, A. J. H. *J. Chem. Phys.* **1970**, *52*, 1033−1036. Wachters, A. J. H. *IBM Technol. Rep. RJ584* **1969**.

(35) Basis sets were obtained from the Extensible Computational Chemistry Environment Basis Set Database, Version 1.0, as developed and distributed by the Molecular Science Computing Facility, Environmental and Molecular Sciences Laboratory, which is part of the Pacific Northwest National Laboratory, P.O. Box 999, Richland, WA 99352, and is funded by the U.S. Department of Energy under contract DE-AC06-76RLO 1830. Contact David Feller, Karen Schuchardt, or Don Jones for further information.

(36) Perdew, J. P.; Wang, Y. *Phys. Rev. B* **1992**, *45*, 13244−13249.

(37) Frisch, M. J.; Trucks, G. W.; Schlegel, H. B.; Gill, P. M. W.; Johnson, B. G.; Robb, M. A.; Cheeseman, J. R.; Keith, T.; Petersson, G. A.; Montgomery, J. A.; Raghavachari, K.; Al-Laham, M. A.; Zakrzewski, V. G.; Oritz, J. V.; Foresman, J. B.; Cioslowski, J.; Stefanov, B. B.; Nanayakkara, A.; Challacombe, M.; Peng, C. Y.; Ayala, P. Y.; Chen, W.; Wong, M. W.; Andres, J. L.; Replogle, E. S.; Gomperts, R.; Martin, R. L.; Fox, D. J.; Binkley, J. S.; Defrees, D. J.; Baker, J.; Stewart, J. P.; Head-Gordon, M.; Gonzalez, C.; Pople, J. A. *Gaussian94*, Revision C.2; Gaussian, Inc.: Pittsburgh, PA, 1995.

(38) Chesnut, D. B.; Moore, K. D. *J. Comput. Chem.* **1989**, *10*, 648−659.

Table 2.   Structural Summary for OEP/TPP Porphyrins[a]

	Fe(OEP)(CO)(1-MeIm)	Ru(OEP)(CO)(1-MeIm)	Os(OEP)(CO)(1-MeIm)	Fe(TPP)(iPrNC)(1-MeIm)
M−N(1)	1.998(3)	2.054(3)	2.063(8)	2.004(4)
M−N(2)	1.998(3)	2.060(3)	2.058(8)	1.994(4)
M−N(3)	2.005(3)	2.063(3)	2.057(8)	1.996(4)
M−N(4)	2.000(3)	2.060(3)	2.061(8)	2.000(4)
M−C	1.744(5)	1.829(5)	1.817(13)	1.847(5)
M−N(base)	2.077(3)	2.192(4)	2.177(9)	2.041(4)
C−O/C−N	1.158(5)	1.156(5)	1.171(13)	1.155(6)
N(1)−M−N(2)	90.03(14)	90.17(12)	89.9(3)	89.89(14)
N(1)−M−N(3)	178.11(13)	175.66(14)	174.1(4)	178.6(2)
N(1)−M−N(4)	89.86(14)	89.75(13)	90.2(3)	89.9(2)
N(2)−M−N(3)	89.79(14)	89.64(13)	89.4(3)	89.9(2)
N(2)−M−N(4)	178.31(13)	175.6(2)	173.9(4)	178.5(2)
N(3)−M−N(4)	90.26(13)	90.11(13)	89.9(3)	90.3(2)
C−M−N(1)	89.8(2)	91.4(2)	94.2(4)	89.9(2)
C−M−N(2)	88.3(2)	90.9(2)	94.2(4)	96.1(2)
C−M−N(3)	92.0(2)	92.9(2)	91.7(4)	91.4(2)
C−M−N(4)	93.4(2)	93.5(2)	91.9(4)	85.3(2)
C−M−N(base)	176.8(2)	178.3(2)	177.9(4)	174.1(2)
M−C−O/M−C−N	175.1(4)	177.3(4)	177.0(9)	170.1(4)
angle between N(base) and porphyrin N−N bond vector	1°	4°	4°	24°
angle between N(base) ring and the porphyrin plane	91°	87°	88°	85°

[a] M: metal center Fe, Os, or Ru as appropriate.

functional was used in each case.[37] Calculations were carried out in this laboratory on International Business Machines (Austin, TX) RS/6000 computers (models 340, 350, 360, 365, and 3CT) and on an 8-processor Silicon Graphics/Cray Research (Mountain View, CA) Origin-200 cluster, and on SGI Origin-2000 and Power Challenge multiple processor machines located at the National Center for Supercomputing Applications, located in Urbana, IL, using up to 16 processors.

Results and Discussion

We have synthesized and elucidated the structures of four new porphyrin compounds: the Fe, Ru, and Os complexes of OEP with 1-methylimidazole and CO as axial ligands, together with the Fe(iPrNC)(1-MeIm) complex of TPP, which enable us to begin to investigate in a systematic way how metalloporphyrins containing different ring and axial ligand substitutions may influence porphyrin distortions, as well as serving as useful model compounds with which to probe metalloprotein structure. The SHELXTL structures of these four molecules are shown in Figure 2, and selected metric details are presented in Table 2. The availability of these new structures now enables a comparison to be made between the structures of the OEP and TPP CO systems and between the CO and RNC TPP systems, and these results, together with those for the OEP and TPP O_2-analogue systems to be described elsewhere,[23] lead to new insights into the likely occurrence of porphyrin (and ligand) distortions in metalloporphyrins.

As may be seen from Figures 3 and 4, there are remarkable differences, as well as remarkable similarities, between the TPP and OEP systems. The largest differences occur in the extent of porphyrin ruffling. In the cases of Fe(TPP)(CO)(1-MeIm), Ru(TPP)(CO)(1-MeIm), and Os(TPP)(CO)(1-MeIm), there are pronounced saddle distortions, with mean absolute deviations of C^β from the least-squares porphyrin plane of $|\overline{C^\beta}| = 0.286$ Å (Fe TPP), $|\overline{C^\beta}| = 0.196$ Å (Ru TPP), and $|\overline{C^\beta}| = 0.183$ Å (Os TPP), to be compared with $|\overline{C^\beta}| = 0.023$ Å (Fe OEP), $|\overline{C^\beta}| = 0.031$ Å (Ru OEP), and $|\overline{C^\beta}| = 0.037$ Å (Os OEP) in the OEP case. In contrast, in the case of Fe(TPP)(iPrNC)(1-MeIm) there
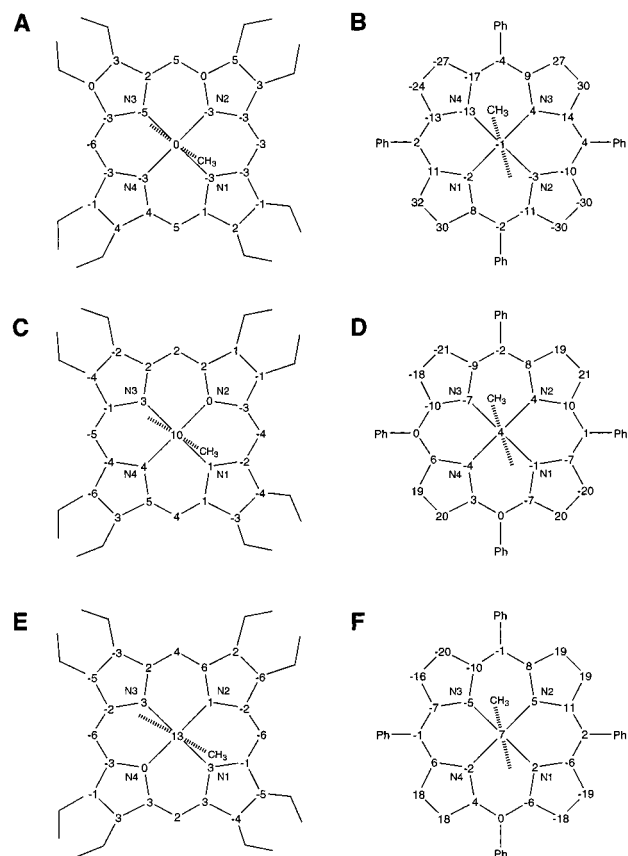

Figure 3.   Schematic illustrations showing atom deviations (in units of 10^{-2}Å) from the least-squares porphyrin plane in several CO metalloporphyrins: (A, C, E) the Fe-, Ru-, Os(OEP)(CO)(1-MeIm) systems described in this paper; (B, D, F) the Fe-, Ru-, Os(TPP)(CO)-(1-MeIm) systems described elsewhere (refs 17 and 50). The TPP derivatives are much more distorted than the OEP derivatives.

is almost no distortion, with $|\overline{C^\beta}| = 0.014$ Å, Figure 4. Differences are also seen in the orientation of the 1-MeIm with respect to the nearest N−N bond vector. The plane of the
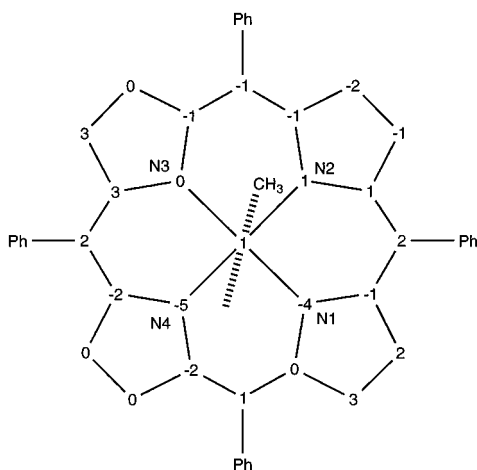
Figure 4. Schematic illustration showing atom deviations (in units of 10^{-2}Å) from the least-squares plane in Fe(TPP)(iPrNC)(1-MeIm). Unlike the CO derivative, the iPrNC system is essentially planar ($|\overline{C^\beta}|$ = 0.014 Å).

imidazole is oriented at $\sim3°$ to the N−N bond vector in the OEP derivatives, Table 2 and (schematically) Figure 3, to be compared with a $\sim30°$ orientation in the TPP CO derivatives, Figure 3, and a $\sim24°$ orientation in Fe(TPP)(iCN)(1-MeIm), Figure 4. These values are similar to those seen in the OEP/TPP−RNO adducts[23] where the imidazole plane is oriented at $\sim8°$ in Fe(OEP)(PhNO)(1-MeIm) but at $\sim27°$ in Fe(TPP)-(PhNO)(1-MeIm). The M−C−O bonds are generally close to linear, although there is a $\sim5°$ distortion in Fe(OEP)(CO)(1-MeIm), Table 2.

The major structural differences observed between the various systems therefore involve porphyrin ruffling and are quite pronounced, and puzzling. If we invoke an electronic origin due to porphyrin substitution, then the TPP CO species might be distorted while the OEP derivatives are not, but the isoelectronic TPP RNC derivative is quite undistorted, Figure 4. Also, we noted previously in the corresponding pyridine adducts, Fe-, Ru-, Os(TPP)(CO)(py), that each system is undistorted.[17] It therefore appears to be necessary to consider the axial base (py TPP CO adducts are planar, 1-MeIm TPP CO adducts are distorted), the axial ligand (TPP CO 1-MeIm is distorted, TPP iPrNC 1-MeIm is planar), as well as the porphyrin substitution pattern, to arrive at a model that can predict, at least qualitatively, the observed trends. While quantum chemical geometry optimizations should in the future permit a more detailed analysis of these observations, for now we focus on the development of a plausible empirical model that predicts the observed results with good accuracy.

An Analysis of Porphyrin Ruffling. As noted above, the four new compounds we have synthesized have planar metalloporphyrins, even though the RNC derivative has a relatively bulky isopropylisocyanide ligand, and phenyl substitutions. The origins of the porphyrin ring distortions are thus not immediately obvious. However, in other work,[23] we have investigated the structures of five additional metalloporphyrins, four of which are O_2-heme analogues, and we have also obtained a high-resolution structure of an additional, distorted carbene system.[39] Three of these six compounds are ruffled and three are not. The three distorted systems are (using the shorthand notation given above and noting that PhNO ≡ nitrosobenzene and NODMA ≡ 4-nitroso-N,N-dimethylaniline) Fe(TPP)(PhNO)-

(39) Salzmann, R.; Ziegler, C.; Suslick, K.; Oldfield, E., unpublished results.

Table 3. Comparison between Experimental Porphyrin C^β Distortions and Prediction

type	system	mean C^β (expt, Å)[a]	distortion prediction[b]
TPP/CO	Fe(TPP)(CO)(1-MeIm)	0.286	+
	Fe(TPP)(CO)(py)	0.049	−
	Ru(TPP)(CO)(1-MeIm)	0.196	+
	Ru(TPP)(CO)(py)	0.04	−
	Os(TPP)(CO)(1-MeIm)	0.183	+
	Os(TPP)(CO)(py)	0.055	−
OEP/CO	Fe(OEP)(CO)(1-MeIm)	0.023	−
	Ru(OEP)(CO)(1-MeIm)	0.031	−
	Os(OEP)(CO)(1-MeIm)	0.037	−
RNC	Fe(TPP)(iPrNC)(1-MeIm)	0.014	−
RNO	Fe(TPP)(PhNO)(1-MeIm)	0.032	−
	FE(TPP)(PhNO)(py)	0.288	+
	Fe(TPP)(NODMA)(py)	0.156	+
	Fe(OEP)(PhNO)(1-MeIm)	0.038	−
5-coordinate	Co(OEP)(NO)	0.047	−
	Fe(TPP)(CCl₂)	0.235	+

^{a} The mean C^β values were for the 14 structures determined in this laboratory, together with the structures of Fe(TPP)(CO)(py) and Ru(TPP)(CO)(py) reported in refs 49 and 50. ^{b} Predictions were made by using the logic-based model described in the text: $f(A,B,C) = A{\bullet}B{\oplus}C$, where A represents the presence of a ring phenyl group, B indicates the presence of a large or "distorting" axial subsituent (including 1-MeIm), and C is a small or "nondistorting" ligand. Note the presence of two distorting axial ligands results in no net distortion.

Using a cutoff of $|\overline{C^\beta}| \geq 0.06$ Å to indicate the presence of ruffling, there is a 1:1 correlation between experiment and prediction.

(py), Fe(TPP)(NODMA)(py), and Fe(TPP)(CCl₂), while the three unruffled systems are Fe(TPP)(PhNO)(1-MeIm), Fe(OEP)-(PhNO)(1-MeIm), and Co(OEP)(NO).[23]

While these results may at first all appear unrelated, we can in fact now begin to develop a predictive model for ruffling, based on the following observations: First, of the 16 compounds considered here and elsewhere, ruffling is only seen in the TPP series, although it is not always present, Table 3. There are 6 out of 16 compounds containing large distortions: the three 1-MeIm/CO adducts, the two py/RNO adducts, and Fe(TPP)-(CCl₂). The two 1-MeIm/RNO adducts, unlike the MeIm/CO species, are undistorted, as is the other five-coordinate species, Co(OEP)(NO). These results suggest the following rule: that in order for there to be a porphyrin distortion there needs to be one and only one repulsive interaction between a porphyrin ring substituent and an axial ligand. This can be expressed symbolically by the logical operation: $f(A,B,C) = A{\bullet}B \oplus C$ where A, B, C represent the presence or absence of a particular group, with A representing the ring substitution. The dot (•) represents a logical AND statement and the $\oplus$ an exclusive OR statement. Sixteen out of sixteen porphyrin distortions considered can be predicted by dividing the axial/equatorial substituents into two classes: 1 = PhNO, NODMA, CCl₂, 1-MeIm, *ring*-phenyl, and 0 = CO, NO, pyridine, *ring*-ethyl. For example, for A = Ph = 1, B = CO = 0, and C = py = 0, the operation A•B $\oplus$ C yields $f(A,B,C) = 0$, or no ring distortion. For A = Ph = 1, B = CO = 0, and C = 1-MeIm, $f(A,B,C) = 1$, ruffling is predicted. For A = Ph = 1, B = PhNO = 1, and C = py = 0, $f(A,B,C)$ = 1, ruffling is predicted. For A = Ph, B = PhNO, and C = 1-MeIm, $f(A,B,C) = 0$, no distortion, and so forth, as shown in Table 3. To what extent these effects are purely inter-/intramolecular steric or electronic is unknown, and will have to be determined in the future by using quantum chemical geometry optimization methods, possibly on both single molecules and with periodic boundary conditions, on crystal lattices.[40] But qualitatively, the picture that emerges from the above analysis is very simple and is that ring distortions due to
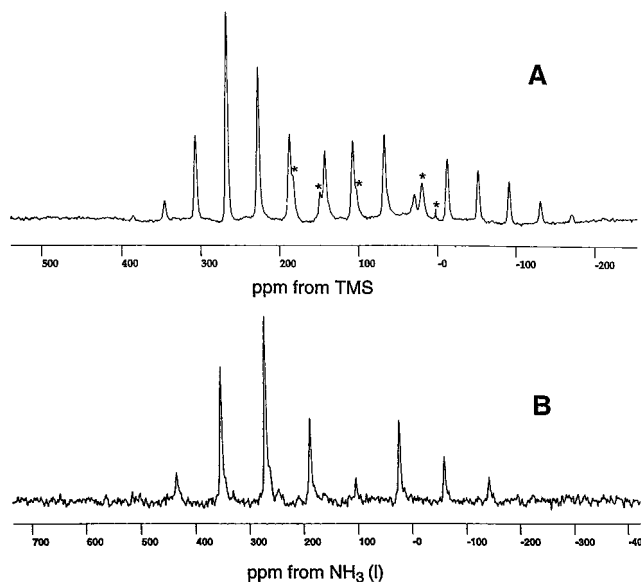
Figure 5. Typical CP-MAS NMR spectra: (A) 8.45 T ^{13}C CP-MAS NMR spectrum of Os(OEP)(^{13}CO)(1-MeIm), 5.0 kHz spin speed, 4720 scans at a 3 s recycle time and (B) ^{15}N MAS NMR spectrum of Fe-(TPP)(iPr^{15}NC)(1-MeIm), 2.5 kHz spin speed, 7040 scans at a 2 s recycle time. The asterisks in part A arise from the OEP porphyrin carbons.

axial ligation differences are only seen when the ligation pattern involves **one** large or distorting ligand, interacting with a large ring substituent. When two such axial ligands are present, the distortions cancel, as indicated logically with the A•B ⊕ C operation. The effect certainly appears steric, as evidenced by the increased size of the A-type ligands listed above, with 1-MeIm being in the A-class due to its somewhat angular substitution pattern. On the basis of the results shown in Table 3, the predictions are quite robust: for all six distortion predictions ("+" in Table 3) the $|\overline{C^\beta}|$ value is on average 0.22 Å, to be compared with $|\overline{C^\beta}| = 0.04$ Å for the 10 nondistorted predictions ("−" in Table 3).

Solid-State NMR and Quantum Chemistry. We next carried out a ^{13}C, ^{15}N, and ^{17}O nuclear magnetic resonance spectroscopic investigation of ^{13}CO, C^{17}O, iPrN^{13}C, and iPr-^{15}NC labeled metalloporphyrins, using "magic-angle" sample spinning (MAS). We also used density functional theory to predict these same parameters, which provides a test of our ability to predict spectroscopic observables in relatively well characterized materials. Testing the theoretical methods on heme model compounds is of importance since it can give enhanced confidence in the reliability of the calculations themselves, or more precisely, in the values of properties such as the charge density, ($\rho(\mathbf{r})$), the electrostatic potential ($\Phi(\mathbf{r})$), and the electric field gradient ($\nabla\bullet E$), which can also be independently deduced in some cases from diffraction data,[41–43] as well as $\nabla^2\rho(\mathbf{r})$, of interest in the context of chemical and hydrogen bonding[44]—a long-term objective of this research.

(40) Marchi, M.; Hutter, J.; Parrinello, M. *J. Am. Chem. Soc.* **1996**, *118*, 7847−7848. Rovira, C.; Kune, K.; Hutter, J.; Ballone, P.; Parrinello, M. *J. Phys. Chem. A* **1997**, *101*, 8914−8925.

(41) Koritsánszky, T.; Flaig, R.; Zobel, D.; Krane, H.-G.; Morgenroth, W.; Luger, P. *Science* **1998**, *279*, 356−358.

(42) Flaig, R.; Koritsanszky, T.; Zobel, D.; Luger, P. *J. Am. Chem. Soc.* **1998**, *120*, 2227−2238.

(43) Coppens, P. *X-ray Charge Densities and Chemical Bonding*; Oxford University Press: New York, 1997.

(44) Bader, R. F. W. *Atoms in Molecules. A Quantum Theory*; Clarendon Press: Oxford, 1990.
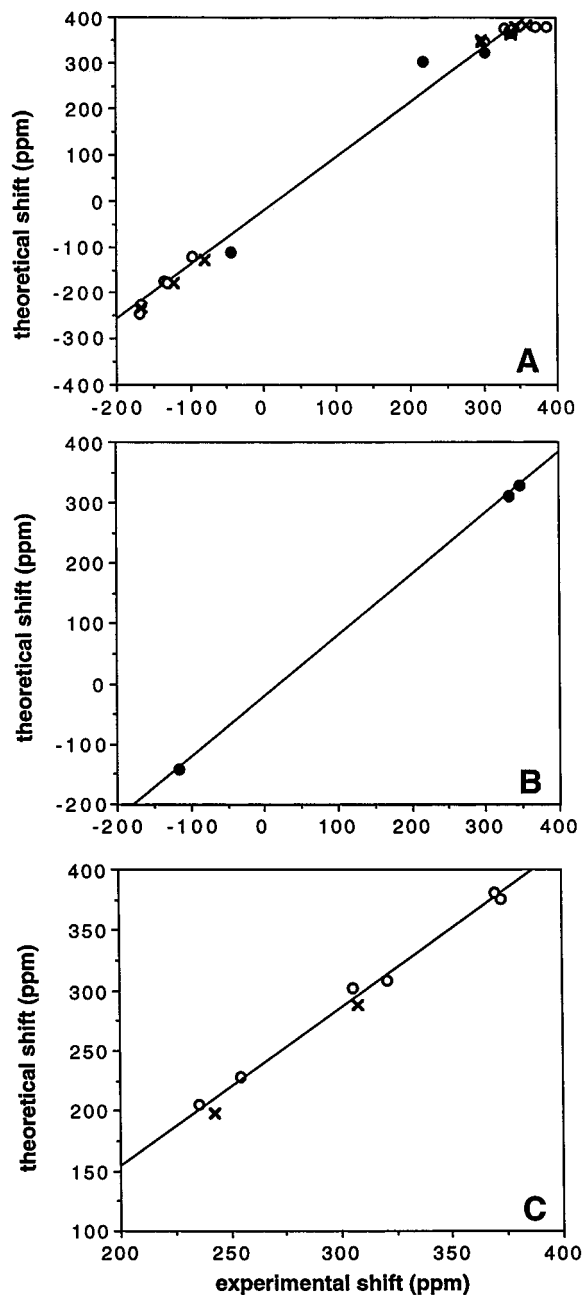
Figure 6. Graph showing experimental versus theoretical shifts and shift tensor elements for the compounds investigated. (A) Graph showing correlations for carbon-13 tensor elements (slope = 1.18, R^2 = 0.99): (○) TPP metalloporphyrin complexes from ref 17; (×) OEP metalloporphyrin complexes (data from Table 4); (●), Fe(TPP)(iPrNC)-(1-MeIm) (data from Table 4). (B) Graph showing correlations for nitrogen-15 tensor elements (slope = 1.01, R^2 = 1.0) for Fe(TPP)-(iPrNC)(1-MeIm). (C) Graph showing correlations for oxygen-17 isotropic shifts (slope = 1.32, R^2 = 0.99): (○) TPP complexes from ref 17; (×) OEP complexes (Table 4). The line is drawn through all of the data points.

We show in Figure 5 representative ^{13}C and ^{15}N CP-MAS NMR spectra, in this case of Os(OEP)(^{13}CO)(1-MeIm) and Fe-(TPP)(iPr^{15}NC)(1-MeIm). Additional spectra of these and the other compounds were also obtained at different spinning speeds, and the principal components of the chemical shift tensor, δ_{ii}, were derived by using the Bayesian probability/Herzfeld−Berger method[45] described elsewhere.[46] A compilation of the experimental results is given in Table 4. For the ^{17}O spectra of the

(45) Herzfeld, J.; Berger, A. *J. Chem. Phys.* **1980**, *73*, 6021−6030.

Table 4. Comparison of Experimental NMR Chemical Shifts and Chemical Shift Tensor Elements with Theoretical Values, for CO and iPrNC Model Systems[a,b]

system		δ_{iso} (ppm)	δ_{11} (ppm)	δ_{22} (ppm)	δ_{33} (ppm)	$\|\delta_{33} - \delta_{11}\|$ (ppm)
Fe(OEP)(^{13}CO)(1-MeIm)	expt	206.9	358	343	−83	441
	calc	215	385	383	−123	508
Fe(OEP)(C^{17}O)(1-MeIm)	expt					
	calc	376	635	634	−142	777
Ru(OEP)(^{13}CO)(1-MeIm)	expt	183	336	336	−124	460
	calc	188	370	368	−174	544
Ru(OEP)(C^{17}O)(1-MeIm)	expt	307				
	calc	290	558	557	−244	802
Os(OEP)(^{13}CO)(1-MeIm)	expt	141	296	296	−169	465
	calc	159	352	350	−227	579
Os(OEP)(C^{17}O)(1-MeIm)	expt	242				
	calc	199	507	504	−416	923
Fe(TPP)(iPrN^{13}C)(1-MeIm)	expt	158				
	calc	174	325	306	−108	432
Fe(TPP)(iPr^{15}NC)(1-MeIm)	expt	186	346	330	−118	464
	calc	168	331	312	−138	469
Fe(TPP)(iPrN^{13}C)(py)[c]	expt	151				
Fe(TPP)(iPr^{15}NC)(py)[c]	expt	188	357	332	−125	482
sperm whale[d] Mb•iPrN^{13}C	expt	173.4				
adult human[d] Hb•iPrN^{13}C[d] site 1	expt	177.3				
site 2	expt	178.0				
rabbit Hb•iPrN^{13}C site 1	expt	170.4				
site 2	expt	176.9				

[a] The theoretical chemical shieldings (σ) were converted to theoretical chemical shifts ("calc" in the table) by using the following absolute shieldings: ^{13}C, δ(^{13}C, TMS) ppm = 186.5 − σ (ref 51); ^{15}N, δ(^{15}N, NH$_3$) ppm = 244.6 − σ (ref 52), and for ^{17}O, δ(^{17}O,H$_2$O) ppm = 306.7 − σ (ref 53). [b] Shielding calculations were typically performed by using the G94/DFT/GIAO Fe Wachters'/6-311++G(2d)/6-31G∗/3-21G∗/BPW91 approach with crystallographic structures: see the text for more details. [c] The structure of this compound was not solved so only the experimental shift results are shown. [d] Reference 48.

CO species and the ^{13}C spectrum of Fe(TPP)(iPrN^{13}C)(1-MeIm), only the isotropic shifts are reported, due to weak signal-to-noise ratios and quadrupolar effects. Our ^{13}C isotropic shift for the Fe(TPP)(iPrNC)(py) compound is essentially the same as that determined previously by Morishima et al. for a (reported) bis-isocyanide TPP complex,[47] but we believe that their compound was actually the mono-pyridine adduct, since it has the same chemical shift as our Fe(TPP)(iPrNC)(py), and their solvent was pyridine. For both the ^{13}CO and R^{15}NC shielding tensors, we find good accord between theory and experiment for each of the individual tensor elements, Table 4 and Figures 6A,B. This result was expected for the Fe, Ru, Os systems, based on the results found previously for Fe-, Ru-, Os(TPP)(CO)(1-MeIm),[17] but no shielding calculations have been reported for RNC−metalloporphyrins. In addition, C^{17}O isotropic shieldings are quite well predicted, Figure 6C. For the essentially linear and untilted Fe−, Ru− and Os−^{13}CO compounds, we find that there is very close to axial symmetry in both the experimental shielding tensor elements and the calculations, Table 4. More surprisingly, the ^{15}N shielding tensor, both experimentally and theoretically, is also very close to being axially symmetric, with σ_{ii} = 346, 330, and −118 ppm (expt) and σ_{ii} = 331, 312, and −138 ppm (calc), with overall tensor spans of 464 (expt) and 469 (calc). As discussed elsewhere, errors in the absolute shielding in such systems (for ^{13}C, ^{15}N, and ^{17}O) are expected to be ∼10−20 ppm.[17]

In sperm whale myoglobin and in adult human and rabbit hemoglobin RNC adducts, there are, however, considerable shielding differences to those seen with the model compound.[48] In particular, the iPrN^{13}C shift in the proteins is some 15−20 ppm downfield from that observed in the model compound, a major change from the small shielding differences seen previously between model ^{13}CO-containing compounds and metalloproteins, which are typically only ∼2 ppm.[17] One possible explanation for this unusual finding might be that the RNC group has been reported to display a large range of tilt (τ) and bend (β) angles in proteins,[21,22] where τ and β are as shown below:
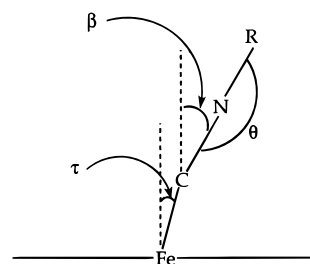
In addition, large distortions at nitrogen in the alkylisocyanide adducts of myoglobin and hemoglobin have been reported,[21,22] and might also influence shielding. For example, C′NR bond angles (θ, above) from 145.6 to 96.0° have been noted and

(46) Havlin, R. H.; McMahon, M.; Srinivasan, R.; Le, H.; Oldfield, E. *J. Phys. Chem.* **1997**, *101*, 8908−8913.

(47) Morishima, I.; Hayashi, T.; Inubushi, T.; Yonezawa, T.; Uemura, S. *J. Chem. Soc. Chem. Commun.* **1979**, 483−485.

(48) Mansuy, D.; Lallemand, J.-Y.; Chottard, J.-C.; Cendrier, B.; Gacon, G.; Wajcman, H. *Biochem. Biophys. Res. Commun.* **1976**, *70*, 595−599. Dill, K.; Satterlee, J. D.; Richards, J. H. *Biochemistry* **1978**, *17*, 4291−4297. Stetzkowski, F.; Banerjee, R.; Lallemand, J.-Y.; Cendrier, B.; Mansuy, D. *Biochimie* **1980**, *62*, 795−801.

(49) Peng, S.-M.; Ibers, J. A. *J. Am. Chem. Soc.* **1976**, *98*, 8032−8036.

(50) Little, R. G.; Ibers, J. A. *J. Am. Chem. Soc.* **1973**, *95*, 8583−8590. Slebodnick, C.; Seok, W. K.; Kim, K.; Ibers, J. A. *Inorg. Chim. Acta* **1996**, *243*, 57−65.

(51) Jameson, K. J.; Jameson, C. J. *Chem. Phys. Lett.* **1987**, *134*, 461−466.

(52) Jameson, C. J.; Jameson, A. K.; Oppusunggu, D.; Willie, S.; Burrell, M.; Mason, J. *J. Chem. Phys.* **1981**, *74*, 81−88.

(53) Wasylishen, R. E.; Mooibroek, S.; Macdonald, J. B. *J. Chem. Phys.* **1984**, *81*, 1057−1059.
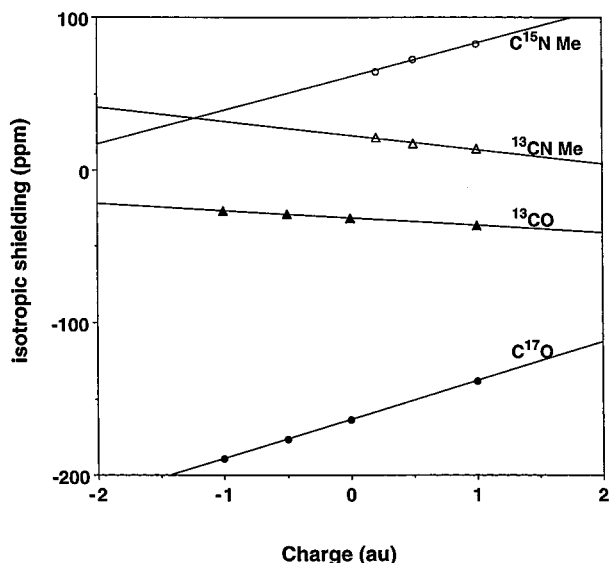
Figure 7. Electrostatic field contributions to shielding in [FeCO](2e) and [FeCNMe](2e) model systems. ▲, ^{13}CO; △, $CH_3N^{13}C$; ●, $C^{17}O$; and ○, $CH_3^{15}NC$. The isotropic chemical shifts are shown as a function of the size of the charge placed 4.45 Å distal to the terminal O, N atoms, along the Fe−C bond axis. ^{13}CO slope = 4.6 ppm/au, R^2 = 1.0; $CH_3N^{13}C$ slope = −9.0 ppm/au, R^2 = 0.99; $C^{17}O$ slope = 25.4 ppm/au, R^2 = 1.0; $CH_3^{15}NC$ slope = 22.1 ppm/au, R^2 = 1.0.

rationalized in terms of the existence of the Pauling valence forms:

$$Fe \leftarrow C \equiv N\text{-}R \longleftrightarrow Fe = C = N_{\searrow R}$$
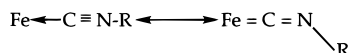
Unfortunately, it is not at present very realistic to expect to reliably evaluate these protein shieldings, since there are too many structural uncertainties. Indeed, as with our previous work on ^{13}C, ^{17}O NMR of CO-heme proteins,[18−20] use of the reported X-ray structures does not give good agreement with experiment (data not shown). It is, however, of interest to try to assess which factors are most likely to influence isocyanide shielding and energetics in proteins, since this approach could lead to ruling out some explanations while favoring others.

We therefore first investigated the sensitivity of both ^{13}C and ^{15}N shieldings to electrostatic field effects, using the [FeCNMe](2e) cluster shown in Figure 1A, and the same basis sets as reported previously by deDios and Earle.[27] Since linear relationships between charge and shift are expected,[27] only a limited number of points were evaluated, and these results are shown, together with a corresponding set of results for [FeCO](2e), in Figure 7. There is the expected anti-correlation between $RN^{13}C$ and R^{15}-NC shieldings (due to polarization) as a function of the electrostatic field (the value of the external charge), with a close correspondence between the results for the two systems. This strongly suggests that it is most unlikely that electrostatic field effects alone could be responsible for the ^{13}C chemical shift changes seen between the model compound and the metalloproteins, since in the presence of a similar local charge field to that present in the CO-heme proteins,[27] ^{13}C shift changes of only a few ppm would be anticipated, not the 15−20 ppm seen experimentally. More pronounced structural differences are, therefore, indicated.

We consequently evaluated tilt−bend (τ,β) energy and shielding surfaces for the model system shown in Figure 1B, to see to what extent such distortions are permissible, and to what extend they could contribute to the shielding changes seen
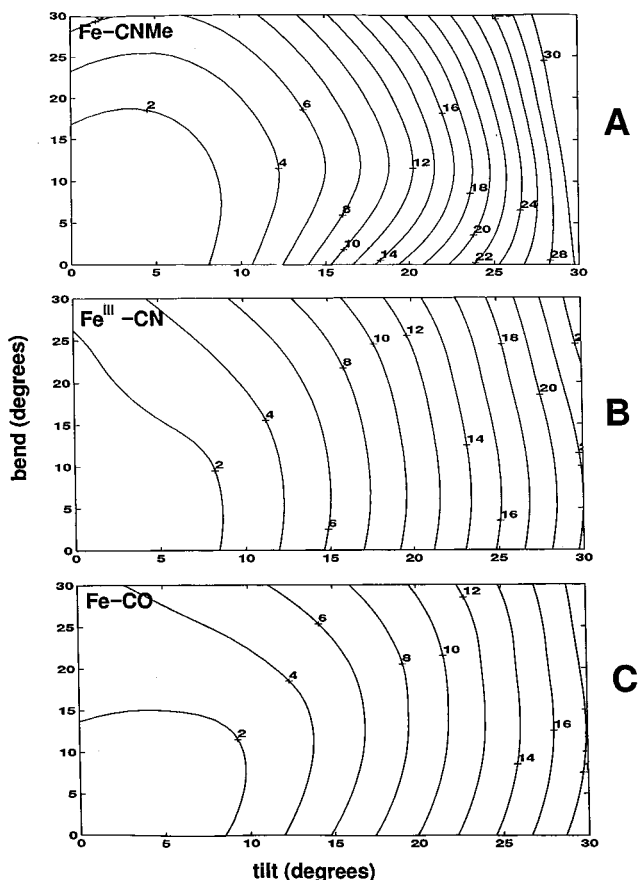

Figure 8. Ligand τ,β energy surfaces for three model metalloporphyrin systems. (A) Fe(bis(amidinato))(MeNC)(Im), this work. (B and C) Energy surfaces for the $Fe^{III}CN$ (B) and Fe(CO) (C) derivatives, based on the work of Vangberg et al.[30] The contour values are in kcal/mol. The RNC derivative is most sensitive to both tilt and bend, CO the least. The energy penalties at large τ,β with the isocyanides make such distortions less likely in metalloproteins.

experimentally. The τ,β energy surface for the Fe(bis(amidinato))(MeNC)(Im) model is shown in Figure 8, together with the corresponding Fe^{III}(bis(amidinato))(CN^-)(Im) and Fe(bis-(amidinato))(CO)(Im) surfaces reported previously by Vangberg and co-workers.[30] As anticipated, ligand tilt (τ) plays the major role in controlling energetics, since both σ and π^* effects will be strongly affected by moving the nearest neighbor C atom off of the heme normal. That is, σ bonding will greatly decrease as C moves away from the p_z, d_z^2 orbitals, while bending (at C) has a much less pronounced effect, as with CO.[30] For $\tau \lesssim 15°$, the τ,β energy surfaces for all three systems are very similar, but at high τ, the RNC energies are larger than those seen in the CO, CN surfaces, making large τ,β inaccessible. Significantly though, from the perspective of chemical shielding, increasing τ,β causes a uniform *increase* in ^{13}CNR shielding, the same effect as that seen previously for the Fe−CO containing systems,[20] but the opposite of the model compound → protein result seen experimentally. For example, for $\tau = 30°$, $\beta = 0°$, we find for the isocyanide adduct a 10 ppm increase in shielding, which is to be compared with the 12.2 ppm result found with the CO adduct. Neither tilt nor β-bend therefore appear to be responsible for the large deshieldings seen in the metalloproteins. The only other likely solution, therefore, appears to be one in which a θ-bend (at N) is involved. We first carried out a test calculation at $\tau = \beta = 0°$, $\theta = 128°$, a structure close to that of the bent Pauling valence form shown above. We found a 46 ppm *deshielding*, a major effect that can

CO-Heme Analogue Structures

J. Am. Chem. Soc., Vol. 121, No. 16, 1999 3827

Table 5. Computed ^{13}C, ^{15}N Shieldings (ppm) and Energies (kcal) for Fe(bis(amidinato))(RNC)(Im) Model Compounds[a]

ligand	τ,β,θ (deg)[b]	^{13}C					^{15}N					E[c]
		σ_i	σ_{11}	σ_{22}	σ_{33}	$\|\sigma_{33}-\sigma_{11}\|$	σ_i	σ_{11}	σ_{22}	σ_{33}	$\|\sigma_{33}-\sigma_{11}\|$	
MeNC	(0,0,180)	6	−117	−105	242	359	116	−3	6	344	347	0.0
	(0,10,180)	7	−117	−105	243	360	116	−7	6	347	354	0.66
	(0,20,180)	8	−116	−104	245	361	115	−18	7	355	373	2.90
	(0,30,180)	11	−114	−102	247	361	114	−36	9	368	404	6.88
	(10,0,180)	7	−117	−105	242	359	116	−1	11	339	340	3.42
	(10,10,180)	7	−116	−102	241	357	117	0	13	338	338	2.65
	(10,20,180)	9	−115	−99	240	355	117	−2	11	342	344	4.00
	(10,30,180)	10	−113	−94	240	353	116	−12	9	350	362	7.31
	(20,10,180)	9	−114	−97	238	352	120	0	41	318	318	11.74
	(20,20,180)	10	−115	−90	236	351	119	2	38	316	314	13.39
	(20,30,180)	11	−114	−84	233	347	115	−1	26	321	322	18.24
	(30,0,180)	16	−101	−86	234	335	119	−9	98	268	277	30.35
	(30,10,180)	16	−98	−86	233	331	117	−6	98	258	264	31.87
	(0,0,170)	3	−123	−109	242	365	114	−5	3	344	349	0.20
	(0,0,160)	−4	−140	−113	241	381	110	−19	5	344	363	0.47
	(0,0,150)	−15	−167	−118	240	407	105	−40	13	343	383	1.37
	(0,0,140)	−28	−200	−123	237	437	98	−66	23	340	406	2.68
	(0,0,130)	−43	−234	−128	232	466	91	−96	37	333	429	5.46
	(0,0,120)	−57	−265	−133	226	491	84	−126	54	325	451	9.32
	(0,0,110)	−67	−283	−136	220	503	79	−153	75	315	468	16.03

[a] Chemical shieldings were evaluated with the deMon/MASTER−CS program (refs 31−33), as described previously for the carbonmonoxy system (ref 20). [b] The tilt (τ), C-bend (β), and N-bend (θ) distortions are in degrees and are as shown in the text. [c] The energies shown are energy differences with respect to the $\tau = \beta = 0°$, $\theta = 180°$ (linear) conformer, in kcal/mol.
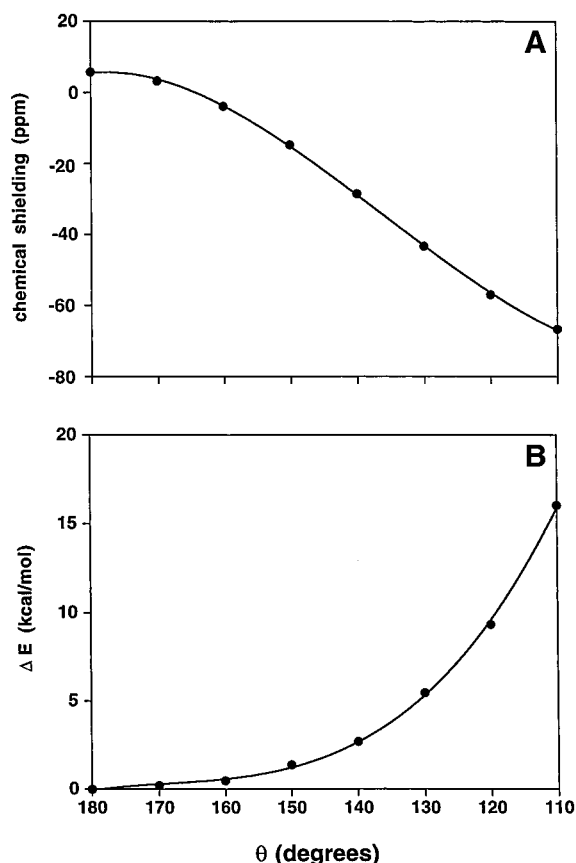

Figure 9. ^{13}C, ^{15}N shielding and energy changes as a function of the N-bend (θ) in the Fe(bis(amidinato))(MeNC)(Im) model compound: (A) ^{13}C shielding and (B) change in energy.

be qualitatively related to the carbene-like nature of the Fe= C−NR tautomer. For example, the ^{13}C shielding in the true carbene Fe(TPP)(CCl$_2$) is at ∼225 ppm downfield from TMS,[39] a very large change from that seen in the RNC model system. This expectation is borne out by the more detailed results presented in Table 5 and in Figure 9, which show the ^{13}C shielding and energetics as a function of the θ-bend angle. A

θ-bend distortion of ∼30° ($\theta = 150°$), corresponding to only a ∼1.5 kcal distortion, would be quite sufficient to explain the protein shift seen experimentally.

Conclusions

The results we have presented above are of interest for a number of reasons. First, they represent the first detailed comparative study of the structures of six-coordinate CO-liganded octaethyl- and tetraphenylporphyrins. The results show that all three OEPs are planar, while the analogous TPP derivatives are ruffled.[17] Second, we have reported the first example of an RNC/1-MeIm metalloporphyrin, a model for alkyl isocyanides bound to heme proteins. The porphyrin here is planar, even though TPP and 1-MeIm are present. Third, we have presented a logic-based approach that successfully predicts the presence of porphyrin distortions in 16 out of 16 CO, RNC, NO, CCl$_2$, RNO containing OEP/TPP metalloporphyrins. Fourth, we have obtained ^{13}C, ^{15}N, and ^{17}O solid-state NMR spectra of the four new metalloporphyrins, and used DFT methods to successfully reproduce the experimental spectra. An interesting observation is that the ^{13}C shift in iPrNC containing metalloproteins is ∼18 ppm deshielded from that observed in the synthetic model compound. DFT calculations rule out electrostatic field effects or Fe−C−N tilt/bend, but a bend at nitrogen in the proteins, such as is present in one of the Pauling valence forms, would introduce carbene-like character, resulting in deshielding at carbon, as observed experimentally.

Salzmann et al.

Supporting Information Available: Tables of crystal data, structure solution and refinement, atomic coordinates, anisotropic displacement parameters, hydrogen coordinates, bond lengths and angles, and torsion angles (PDF). X-ray crystallographic files, in CIF format, are also available through the Internet. This material is available free of charge via the Internet at http://pubs.acs.org.

JA9832818